Experimental Identification of Dynamic Coefficients of Fluid Film Bearings by Using Electro-Magnetic Actuator

Thibaud Plantegenet[1], Mihai Arghir[1], and Jarir Mahfoud[2]

[1] Pprime Institute, CNRS UPR 3346, Université de Poitiers, ENSMA, Chasseneuil du poitou, France
thibaud.plantegenet@univ-poitiers.fr
mihai.arghir@univ-poitiers.fr
[2] Univ. Lyon, INSA-Lyon, CNRS UMR 5259, LaMCos, Villeurbanne F-69621, France
jarir.mahfoud@insa-lyon.fr

Abstract

The present study is focused on the design and use of an Electro-Magnetic Actuator (EMA) for the experimental identification of cylindrical and tilting pad journal bearings rotordynamic coefficients. First, the experimental apparatus is described, then the force-current formulation controlling the EMA is adapted and experimentally validated using the transverse momentum of inertia of the rotor. Finally, an extensive set of experiments is conducted to compute the rotordynamic coefficients of fluid film bearings by resolving a 2 dof system.

1 Introduction

A wide range of rotating machines operate with rotors supported by fluid film journal bearings, especially in high rotational speed or high static/dynamic loads applications. These journal bearings have a large influence on the dynamic of the system. For this reason, it is mandatory to know as accurate as possible the characteristics of the fluid film bearings.

The characteristics of fluid film bearings are governed by a large number of parameters such as fluid viscosity, surface deformations, cavitation. Moreover, the relationship between journal displacements/velocities and the reacting forces is non-linear. The accurate prediction of the characteristics of journal bearings is therefore difficult. One of the main common assumption is to consider small perturbations displacements of the journal. This enables the estimation of the forces transmitted to the rotor by the bearing via rotordynamic coefficients of stiffness, damping and (in cases where inertia forces are important) added mass.

Several experimental methods are available to estimate these coefficients. All are based on the identification of the relationship between an excitation applied to the rotor-bearing system and the measurement of the response. This identification is often made in the frequency domain and therefore the response function is called the Frequency Response Function (FRF). Tiwari et al. [15] and Diamond et al. [5] published very detailed reviews on the identification of dynamic coefficients of fluid film bearings.

A relatively low number of publications present the use of magnetic excitation, via Active Magnetic Bearings (AMB) or Electro-Magnetic Actuators (EMA), for the experimental identification of the dynamic coefficients of fluid film bearings

Knopf and Nordmann [9, 10] designed a test rig composed of two AMBs to identify the coefficients of a plain journal bearing operating in turbulent regime. Voigt [16] used a similar test rig to identify the coefficients of a dynamic seal operating with multiphase fluid flow. In these studies, the excitation forces are estimated from the information given by a Hall effect sensor that measures the flux density passing by each pole of the magnets of the actuator. The displacements of the rotor are measured by inductive proximity probes.

A similar architecture was used by Bellabarba et al. [3] for the identification of the dynamic coefficients of an air-lubricated bearing. The forces were measured by sensors located between the bearing housing and the fixed frame.

Studies by Arumugam et al. [2] and Reddy et al. [13] presented the experimental identification of dynamic coefficients of plain and tilting pad journal bearings using an unidirectional electro-magnetic exciter. The test rig was composed of a flexible rotor supported by a rolling elements bearing at its drive end and by the tested fluid film bearing at its non drive end. The exciter was mounted at the rotor mid-length and had a build-in force transducer. The displacements were measured by inductive proximity probes located near the tested bearing.

In the present study, the test rig architecture is similar to [2, 13], except that a rigid rotor and a full EMA (with four exciters) is used. The EMA was specifically designed for an existing test rig that was previously used for other researches on fluid film bearings. The test rig, the bearings, the EMA and the instrumentation are detailed in the following. Then the force-current formulation is modified and explained for the real geometry and positioning. Finally, three different experimentations are presented: the first one is for the calibration of the EMA; the second one for the identification of the dynamic characteristics of a plain journal bearing and the last one for the identification of a tilting pad journal bearing.

2 Test Rig Description

The test rig presented in the Figure 1 is composed of a rigid rotor guided by a ball bearing at its drive end (DE) side and a fluid film bearing at its non-drive end (NDE) side. The rotor is composed of a hollow shaft with inner and outer diameter of 35 and 45 mm, respectively and a heavy disk of 6.4 kg (149 mm outer diameter and 52 mm length) located at its mid-length. It is driven by a 1.8 kW DC motor via a flexible coupling up to 10 krpm. The static loads supported by the ball and the fluid film bearings are 42 N and 45 N, respectively. The architecture of the rig with a bearing stiffness considerably higher at the rotor DE than at its NDE allows the excitation of the conical rigid mode. High amplitudes of vibration are then generated in the fluid film bearing located at the NDE. This test rig architecture was motivated by previous studies of the Morton Effect [11, 12].

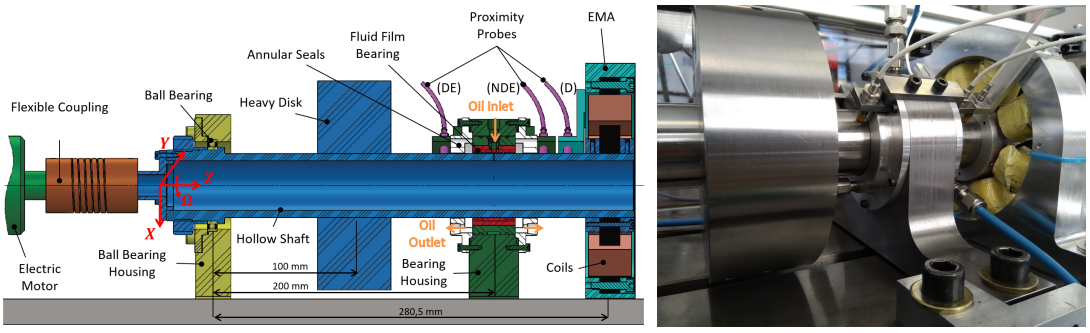

Figure 1: Description of the test rig

2.1 Fluid Film Bearings

Two different fluid film bearings were tested and are presented in the Figure 2: a cylindrical plain journal bearing and a flexure pivot Tilting Pad Journal Bearing (TPJB). The bearings have a L/D ratio of 0.33 and 0.67, respectively. The cylindrical bearing has a radial clearance of 48 µm while the TPJB has a radial bearing clearance of 50 µm and a radial pad clearance of 75 µm. All characteristics

of the TPJB can be found in [12]. Both bearings are supplied with a mineral turbine grade oil ISO VG 32 (kinematic viscosity: 25.1 cP @ 40 °C and 11.5 cP @ 60 °C).

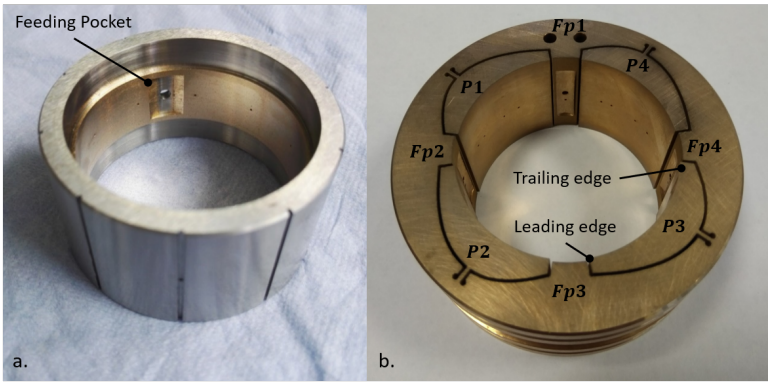

Figure 2: Studied bearings. a. Cylindrical journal bearing. b. Tilting pad journal bearing.

2.2 Electro-Magnetic Actuator Design

The figure 3 presents the EMA that was designed and mounted at the NDE extremity of the test rig. The EMA is composed of eight poles that formed four magnets (I1-I4) regrouped in two axis (I1, I3 on X and I2, I4 on Y). It is specifically designed for the test rig with a dynamic load of 70 N per magnet in order to generate approximately 5 to 10 µm displacements of the journal in the bearing (i.e. 10-20 % of the radial clearance of the bearing). The EMA was also designed very thin in the axial direction for complying the requirements of the test rig. The last specification is the necessity to have a gap much larger than the fluid film bearing radial clearance. This requirement lead to a radial gap of 0.5 mm (10 times the radial clearance of the plain bearing). The design characteristics of the EMA are shown on the Table 1.

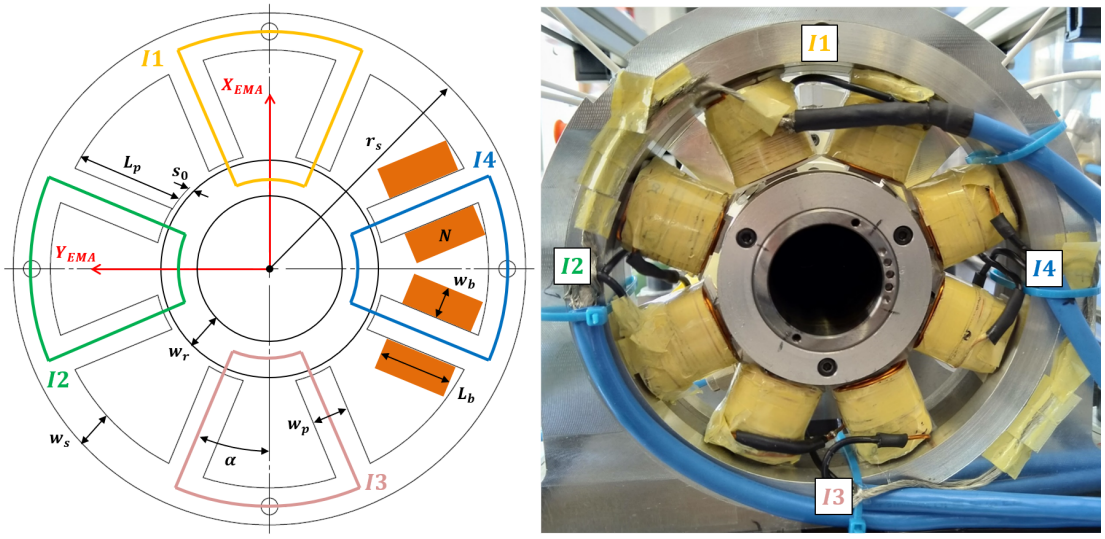

Figure 3: Parameters definition of the EMA and its installation on the test rig.

Geometric parameters		Magnetic parameters	
Radial gap, s_0	0.5 mm	Magnetic induction, B_{sat}/B_{max}	2.2/1.1 T
Pole width, $w_{p,s,r}$	11 mm	Maximum current, i_{max}	7 A
Pole length, L_p	31 mm	Input voltage, U	27.2 V
Pole thickness, e	14.4 mm	Relative permeability, μ_r	2560
Coil width, w_c	8 mm	Coil wire diameter (class)	1.28 mm (16 AWG)
Coil length, L_c	20 mm	Coil turn number, N	126
Pole angle, α	22.5 deg	Theoretic maximum force, f_{max}	140 N
Stator radius, r_s	76 mm		

Table 1: EMA parameters.

As presented in the table 1, the theoretical force for each magnet is 140 N. The selection of this value was based on the requirement of 70 N per magnet with a weighting coefficient of 2. This weighting coefficient was chosen in order to compensate the possible inaccuracies of certain parameters, especially the relative permeability of the ferromagnetic material. A value of 2560 was given by the manufacturer but a lower value of 1100 was experimentally found. This difference affects the force capacity of each magnet. A maximum force value of $f_{max} = 110$ N was found for 7 A and with $\mu_r = 1100$.

2.3 Instrumentation

The test rig is instrumented with 6 proximity probes orthogonally mounted at three different planes: DE side of the fluid film bearing; NDE side of the fluid film bearing and at the EMA (D); the probe planes are located at 165, 235 and 253 mm from the ball bearing centerline, respectively. The current of the EMA is generated by two amplifiers. The amplifiers are controlled by an input voltage comprised between 0 and 10 V. This corresponds to a current generated in the magnets comprised between 0 and 7 A. The current is not directly measured in the EMA but the input voltage of the amplifiers.

3 Force-Current Formulation of the EMA

The force-current formulation of an EMA is taken from Schweitzer et al. [14]. The force generated on an axis line can be expressed as the combination of the opposed magnet forces controlled by the current imposed on each magnet. For a perfectly centered rotor (Figure 4a.), the magnetic force acting on the rotor is described by the equation (1) for both axis (x, y).

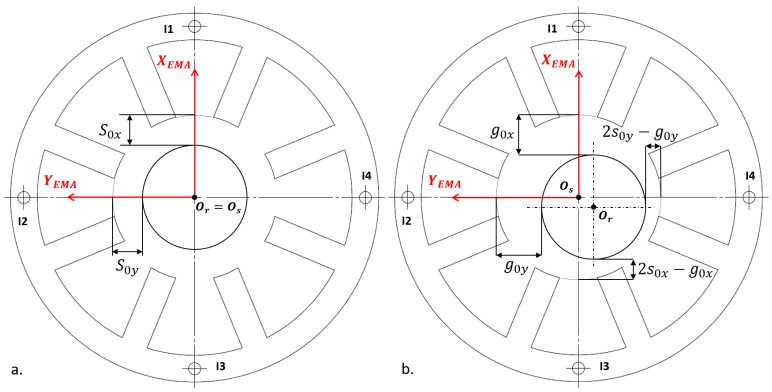

Figure 4: Real radial gap of the EMA for: a. a centered rotor; b. a off-centered rotor.

$$f_{centred_{x,y}} = k^* \left[\frac{(i_0 + i_{x,y})^2}{\left(\frac{l_s+l_r}{\mu_r} + 2(s_{0x,y} - \delta_{x,y})\right)^2} - \frac{(i_0 - i_{x,y})^2}{\left(\frac{l_s+l_r}{\mu_r} + 2(s_{0x,y} - \delta_{x,y})\right)^2} \right] \cos\alpha \tag{1}$$

with $k^* = \mu_0 A N^2$: a constant depending of the parameters of the EMA; $\mu_0 = 4\pi \times 10^{-7}$ Vs/Am: the magnetic permeability of a vacuum; $A = w_p e$: the projected area of a pole; N: the coil turn number; i_0: the bias current; $i_{x,y}$: the control current; $l_s + l_r$: the path of the magnetic circuit on the stator and the rotor; $s_{0x,y}$: the radial gap of the actuator; $\delta_{x,y}$: the displacement of the rotor generated by the control current; and α: the inclination of poles.

The radial gap is theoretically uniform ($s_{0x} = s_{0y} = 0.5$ mm), but this is not true due to machining and mounting tolerances. Experimentally, the radial gap was estimated by successively attracting the rotor (without fluid film bearing) with each magnet and via the measurements of the proximity probes: $s_{0x} = 458.25$ µm and $s_{0y} = 529.75$ µm.

Furthermore, the rotor is never perfectly centered but, as presented on the 4b., it is slightly off-centered due to the fluid film bearing and to the positioning of the EMA on the rig. This off-centered position of the rotor is considered by including the parameter $g_{0x,y}$ in the equation (1) that gives the equation (2).

$$f_{ema_{x,y}} = k^* \left[\frac{(i_0 + i_{x,y})^2}{\left(\frac{l_s+l_r}{\mu_r} + 2(g_{0x,y} - \delta_{x,y})\right)^2} - \frac{(i_0 - i_{x,y})^2}{\left(\frac{l_s+l_r}{\mu_r} + 2(2s_{0x,y} - g_{0x,y} + \delta_{x,y})\right)^2} \right] \cos\alpha \tag{2}$$

The parameter $g_{0x,y}$ is calculated for each test condition based on the real position of the rotor in the stator during the test.

4 Experimental results

4.1 In-Situ Calibration of the EMA

In order to verify the accuracy of the force-current formulation given by the equation (2) an in-situ calibration is required. It is therefore needed to find a measurable parameter that can be verified by other methods. Knopf and Nordmann [9] have calibrated their AMB based on the verification of the properties of the mass of the rotor. In this present work, a similar approach is based on the transverse moment of inertia of the rotor with respect to the center of the ball bearing.

The choice of this parameter is due to the architecture of the test rig that corresponds to a 2dof model, i.e two rotations with respect to the center of the DE ball bearing. This assumption is valid as long as the displacements of the center of the ball bearing are negligibly small. Indeed, the ball bearing has a very high radial stiffness and the rotor behaves as a rigid body for excitation frequencies less than 600 Hz. The transverse moment of inertia with respect to the center of the ball bearing is supposed to be the same along the two axis $J_O = J_{Ox} = J_{Oy}$.

4.1.1 Reference transverse moment of inertia

Several methods can be used to find the value of J_{Oref}, but two of them were chosen for their simplicity: the pendulum theory and the use of CAD software. The pendulum theory is based on equation (3) for small amplitude oscillations ($\sin\alpha = \alpha$).

$$J_{Oref} = \frac{mga}{4\pi^2} T^2 \tag{3}$$

with m: the weight of the rotor; g: the gravitational acceleration, a: the distance between the center of the ball bearing and the center of mass of the rotor; and T: the oscillation period.

Experimentally, the rotor mounted in the ball bearing at the DE was suspended. Several measurements of the oscillation period were recorded with and without the flexible coupling. The transverse moment of inertia estimated by this method was comprised between 0.0646 and 0.0661 kg.m^2. Following a CAD model, the transverse moment of inertia is 0.0687 ans 0.0698 kg.m^2 without and with coupling, respectively. The coupling has not a large influence, but the CAD model gives a slightly higher transverse moment of inertia than the pendulum experiment. This can be explained by the differences between the CAD model and the real rotor but also due to the uncertainty in the pendulum experiment. The values of the transverse moment of inertia were then considered to be between the extreme values, 0.0646 kg.m^2 $< J_{Oref} <$ 0.0698 kg.m^2.

4.1.2 Identification of the transverse moment of inertia with the EMA

A series of tests consisting of sinusoidal excitations of the rotor around an equilibrium position close to the center of the EMA was carried out. The transverse moment of inertia and the excitation intervene in the dynamic equations of motion of the 2 dof model. The fluid film bearing was removed for this tests while the rotor was maintained close to the center of the EMA by a pulley and a counterweight.

The 2 dof model of the rotor, expressed in the frequency domain yields the dynamic stiffness:

$$\begin{cases} \tilde{Z}_x = & \frac{\tilde{F}_{mag_y} l_f}{\tilde{Y}_m} l_m = -\omega^2 J_{O_x} + j\omega C_{O_x} + K_{O_x} \\ \tilde{Z}_y = & \frac{\tilde{F}_{mag_x} l_f}{\tilde{X}_m} l_m = -\omega^2 J_{O_y} + j\omega C_{O_y} + K_{O_y} \end{cases} \tag{4}$$

with $\tilde{Z}_{x,y}$: the dynamic stiffness presenting the FRF between the magnetic forces $\tilde{F}_{mag_{x,y}}$[1] and the displacements $\tilde{X}, \tilde{Y}_m$; $l_f = 280.5$ mm the distance between the EMA and the ball bearing; $J_{0_{x,y}}$: the transverse moments of inertia with respect to the centre of the ball bearing; $K_{O_x,y}$ and $C_{O_x,y}$, the rotational stiffness and damping coefficients (come from the ball bearing and the flexible coupling); ω: the excitation frequency and j the imaginary number ($j^2 = -1$).

The rotations are already replaced in the equation (4)) by using the small perturbation assumption and the measured displacements $\tilde{X}, \tilde{Y}_m$ at the distance $l_m = 253$ mm from the ball bearing center:

$$\begin{cases} \tilde{\psi} = & \arctan\left(-\frac{\tilde{Y}_m}{l_m}\right) & \approx & -\frac{\tilde{Y}_m}{l_m} \\ \tilde{\theta} = & \arctan\left(\frac{\tilde{X}_m}{l_m}\right) & \approx & \frac{\tilde{X}_m}{l_m} \end{cases} \tag{5}$$

The dynamic stiffness can be identified if the magnetic forces are known but as composed of three unknown parameters $J_{O_{x,y}}, K_{O_{x,y}}, C_{O_{x,y}}$ it is not resolvable. However, the dynamic stiffness is complex, thus the real and imaginary parts can be expressed independently:

$$\begin{cases} \Re(\tilde{Z}_x) = & \Re\left(\frac{\tilde{F}_{mag_y} l_f}{\tilde{Y}_m} l_m\right) = & K_{O_x} - \omega^2 J_{O_x} \\ \Re(\tilde{Z}_y) = & \Re\left(\frac{\tilde{F}_{mag_x} l_f}{\tilde{X}_m} l_m\right) = & K_{O_y} - \omega^2 J_{O_y} \end{cases} \tag{6}$$

$$\begin{cases} \Im(\tilde{Z}_x) = & \Im\left(\frac{\tilde{F}_{mag_y} l_f}{\tilde{Y}_m} l_m\right) = & \omega C_{O_x} \\ \Im(\tilde{Z}_y) = & \Im\left(\frac{\tilde{F}_{mag_x} l_f}{\tilde{X}_m} l_m\right) = & \omega C_{O_y} \end{cases} \tag{7}$$

With the imaginary part of $\tilde{Z}_{x,y}$ (7), the rotational damping can be found by knowing the excitation frequency. However, the resolution of the real part of $\tilde{Z}_{x,y}$ is not possible in this state. As dependant

[1] f_{mag} are expressed as the inverse of f_{ema} (eq. 2) due to a change of reference

of the excitation frequency, a set of N measurements with different excitation frequencies allow to solve the system with N equations and two unknown parameters for each axis. This is expressed by the equation (8).

$$\begin{Bmatrix} K_{O_{x,y}} \\ J_{O_{x,y}} \end{Bmatrix} = \begin{bmatrix} 1 & -\omega_1^2 \\ \vdots & \vdots \\ 1 & -\omega_N^2 \end{bmatrix}^{-1} \begin{Bmatrix} \Re(\tilde{Z}_{x,y})_1 \\ \vdots \\ \Re(\tilde{Z}_{x,y})_N \end{Bmatrix} \tag{8}$$

Experimentally, the tests have been performed on the Y axis (rotation around X) for excitation frequencies between 10 Hz and 150 Hz and a variable amplitude of excitation from 2 µm to 7 µm. For each excitation frequency, a set of fifty tests has been conducted to calculate an average value.

The real part of the dynamic stiffness $\Re(\tilde{Z}_x)$ is presented on the Figure 5a. Following the system of equations (8), the rotational stiffness as well as the transverse moment of inertia are identified, $K_{O_x} = 16.64$ Nm/rad $J_{O_x} = 0.0617$ kg.m^2. The Figure 5b. presents the rotational damping C_{O_x}. As expected, the rotational stiffness is low because it is mainly due to the flexible coupling and not due to the ball bearing (the friction in the grease lubricated ball bearing has negligible effect). By comparing J_{O_x} with the reference limits obtained by the pendulum experiment and CAD model, the error is between 4.5 % and 11.6 %. These close results validate the forces in the EMA.

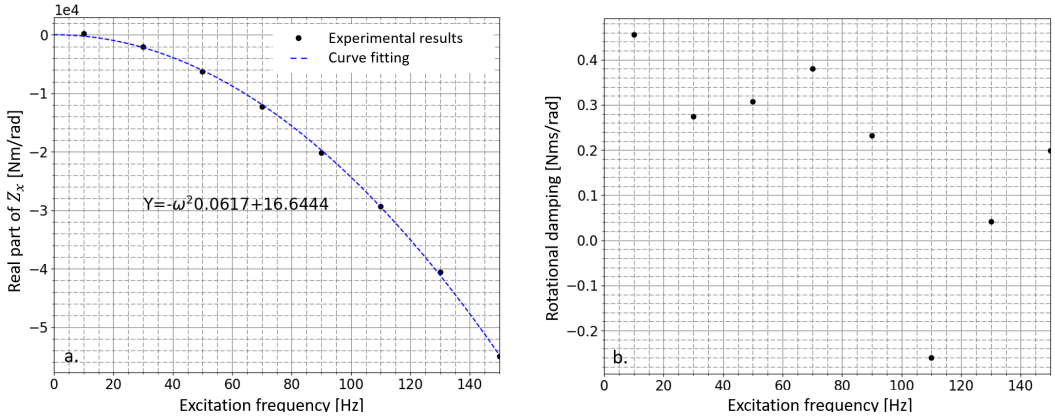

Figure 5: Results of the identification of transverse moment of inertia and the rotational stiffness and damping. a. Real part of the dynamic stiffness. b. Rotational damping.

4.2 Experimental identification of the bearings dynamic coefficients

A similar 2 dof model was used for the identification of the dynamic coefficients of the bearings. This model is valid because the stiffness of the ball bearing is considerably larger than the stiffness of the tested journal bearings. The model of the test rig as well as the main parameters of the 2 dof model are presented on the Figure 6.

The 2 dof in the frequency domain can be expressed:

$$-\omega^2 \begin{bmatrix} J_{O_y} & 0 \\ 0 & J_{O_x} \end{bmatrix} \begin{Bmatrix} \tilde{\theta} \\ -\tilde{\psi} \end{Bmatrix} = \begin{Bmatrix} \tilde{F}_{mag_x} \\ \tilde{F}_{mag_y} \end{Bmatrix} l_f + \begin{Bmatrix} \tilde{F}_{p_x} \\ \tilde{F}_{p_y} \end{Bmatrix} lp \tag{9}$$

with $\tilde{\theta}$ and $\tilde{\psi}$: calculated by the equation (5) and $\tilde{F}_{p_{x,y}}$: the fluid film bearing reaction forces expressed as dynamic coefficients:

$$\begin{Bmatrix} \tilde{F}_{p_x} \\ \tilde{F}_{p_y} \end{Bmatrix} = -\left(\begin{bmatrix} K_{xx} & K_{xy} \\ K_{yx} & K_{yy} \end{bmatrix} + j\omega \begin{bmatrix} C_{xx} & C_{xy} \\ C_{yx} & C_{yy} \end{bmatrix} \right) \begin{Bmatrix} \tilde{X}_p \\ \tilde{Y}_p \end{Bmatrix} = -\begin{bmatrix} \tilde{Z}_{xx} & \tilde{Z}_{xy} \\ \tilde{Z}_{yx} & \tilde{Z}_{yy} \end{bmatrix} \begin{Bmatrix} \tilde{X}_p \\ \tilde{Y}_p \end{Bmatrix} \tag{10}$$

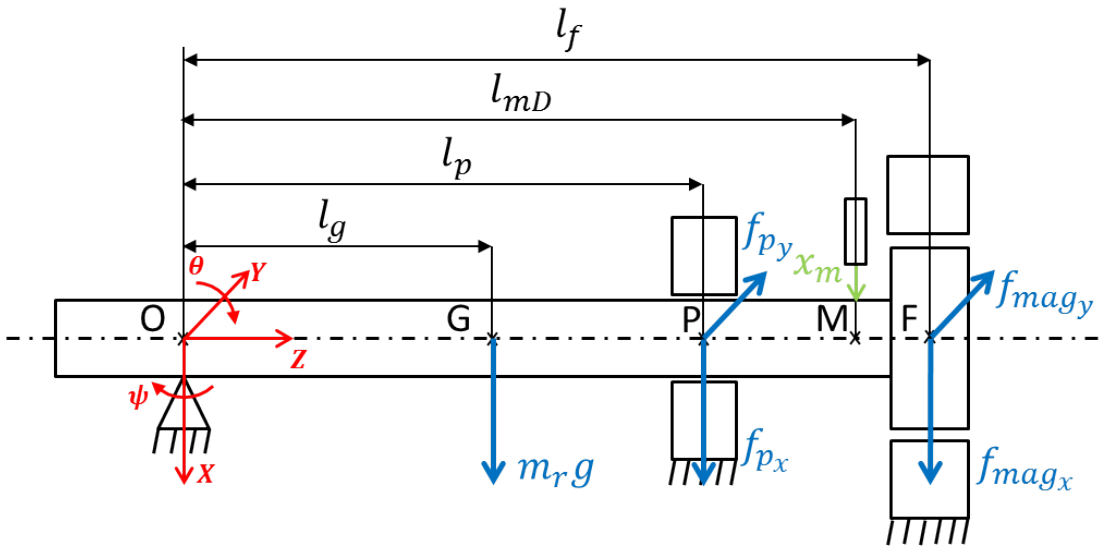

Figure 6: Parameters designation for the 2 dof modelling of the test rig.

with $K_{x,y}$ and $C_{x,y}$ the stiffness and damping of the fluid film bearing, respectively and $\tilde{Z}_{x,y}$: the dynamic stiffness, regrouping both terms. $\tilde{X}_p$, $\tilde{Y}_p$ the displacements in the centre of the bearing and l_p the distance between the fluid film bearing and the ball bearing and expressed in function of the displacement measured at each side of the bearing:

$$\begin{cases} \tilde{X}_p = & \frac{\tilde{X}_{mDE}+\tilde{X}_{mNDE}}{2} \\ \tilde{Y}_p = & \frac{\tilde{Y}_{mDE}+\tilde{Y}_{mNDE}}{2} \end{cases} \tag{11}$$

By replacing the equations (5), (10) and (11) in the equation (9) and by rearranging it gives the equation (12)

$$\begin{bmatrix} \tilde{Z}_{xx} & \tilde{Z}_{xy} \\ \tilde{Z}_{yx} & \tilde{Z}_{yy} \end{bmatrix} \begin{Bmatrix} \tilde{X}_p \\ \tilde{Y}_p \end{Bmatrix} l_p = \begin{Bmatrix} \tilde{F}_{mag_x} \\ \tilde{F}_{mag_y} \end{Bmatrix} l_f + \omega^2 \begin{bmatrix} J_{O_y} & 0 \\ 0 & J_{O_x} \end{bmatrix} \begin{Bmatrix} \tilde{X}_m \\ \tilde{Y}_m \end{Bmatrix} \frac{1}{l_m} \tag{12}$$

The four terms of the dynamic stiffness matrix are unknown and the system have just two equations. By assuming that the equation (12) is true for one test, it is acceptable to assume that another test with an excitation linearly independent from the first one will produce another measure. Thus, it is possible to have two systems of two equations for four dynamic stiffness as presented in the following system of equations (13).

$$\begin{bmatrix} \tilde{Z}_{xx} & \tilde{Z}_{xy} \\ \tilde{Z}_{yx} & \tilde{Z}_{yy} \end{bmatrix} \begin{bmatrix} \tilde{X}_p^{(1)} & \tilde{X}_p^{(2)} \\ \tilde{Y}_p^{(2)} & \tilde{Y}_p^{(2)} \end{bmatrix} l_p = \begin{bmatrix} \tilde{F}_{mag_x}^{(1)} & \tilde{F}_{mag_x}^{(2)} \\ \tilde{F}_{mag_y}^{(1)} & \tilde{F}_{mag_y}^{(2)} \end{bmatrix} l_f + \omega^2 \begin{bmatrix} J_{O_y} & 0 \\ 0 & J_{O_x} \end{bmatrix} \begin{bmatrix} \tilde{X}_m^{(1)} & \tilde{X}_m^{(2)} \\ \tilde{Y}_m^{(1)} & \tilde{Y}_m^{(2)} \end{bmatrix} \frac{1}{l_m} \tag{13}$$

with $\tilde{X}, \tilde{Y}_p^{(1)}$ and $\tilde{X}, \tilde{Y}_m^{(1)}$ the measure of displacements for the first test and similarly for the second test with the exponent (2).

The dynamic stiffness matrix can be computed. However, from a practical point of view, it is not easy to know if two excitations are linearly independent. One way to verify this assumption, is to dissociate the excitation following X from the excitation on Y; i.e. excitation on X: $\tilde{F}_{mag_x}^{(1)} \neq 0$,

$\tilde{F}^{(1)}_{mag_y} = 0$; excitation on Y: $\tilde{F}^{(1)}_{mag_x} = 0$, $\tilde{F}^{(1)}_{mag_y} \neq 0$. This allows to simplified the system of equation (13) to the system (14).

$$\begin{bmatrix} \tilde{Z}_{xx} & \tilde{Z}_{xy} \\ \tilde{Z}_{yx} & \tilde{Z}_{yy} \end{bmatrix} = \left(\begin{bmatrix} \tilde{F}^{(1)}_{mag_x} & 0 \\ 0 & \tilde{F}^{(2)}_{mag_y} \end{bmatrix} \frac{l_f}{l_p} + \omega^2 \begin{bmatrix} J_{O_y} & 0 \\ 0 & J_{O_x} \end{bmatrix} \begin{bmatrix} \tilde{X}^{(1)}_m & \tilde{X}^{(2)}_m \\ \tilde{Y}^{(1)}_m & \tilde{Y}^{(2)}_m \end{bmatrix} \frac{1}{l_m l_p} \right) \begin{bmatrix} \tilde{X}^{(1)}_p & \tilde{X}^{(2)}_p \\ \tilde{Y}^{12)}_p & \tilde{Y}^{(2)}_p \end{bmatrix}^{-1} \tag{14}$$

Similarly to the identification of the transverse moment of inertia of the rotor, the stiffness matrix of the fluid film bearing is obtain from the real part of dynamic stiffness matrix and the damping matrix from the imaginary part.

4.2.1 Application to the plain journal bearing

The plain journal bearing was tested to identify the dynamic coefficients at two different speeds (600 rpm and 3000 rpm) at various excitation frequencies and amplitudes. The experimental results were plotted against a numerical model of the plain journal bearing taking into account the cavitation. However, the numerical model use a simple cavitation model and the small perturbations of the journal are imposed on displacement (on X or Y), while in experiments the force is imposed (on X or Y).

Thirty tests with an excitation on X and thirty tests with an excitation on Y were performed to obtain the experimental dynamic coefficients. This enabled the calculation of 900 results of dynamic coefficients for each frequency and excitation amplitude. The 900 samples follow of a normal distribution. Thus, all the following experimental results are presented as average and standard deviation (error bars) values.

The Figure 7a. presents the comparison of the dynamic coefficients of the plain journal bearing at 600 rpm, for three different excitations frequencies (5, 15 and 35 Hz) and various amplitudes of excitation. The Figure 7b. presents the results at 3000 rpm for excitation frequencies of 10, 30, 60 Hz and various amplitudes of excitation.

The numerical and experimental values are close but the trends are not always the same. Experimentally, all terms of stiffness remain relatively constant with the excitation amplitude (excepting for 35 Hz at 600 rpm). Numerically, these stiffness increase with the excitation amplitude, effect that is more noticeable at super-synchronous excitation frequencies. At 3000 rpm, the direct stiffness are far from the numerical results, especially for 10 Hz. The measured damping coefficients agree well with numerical results excepting for some cross-coupling terms at 600 rpm and for the direct damping at 3000 rpm.

4.2.2 Application to the tilting pad journal bearing

The experimental identification of the dynamic coefficients of the tilting pad bearing is made using the same procedure. The only difference is for the static load of the bearings. To test the tilting pad journal bearing, the heavy disk was removed, thus, the static load of the fluid film bearing was 9 N.

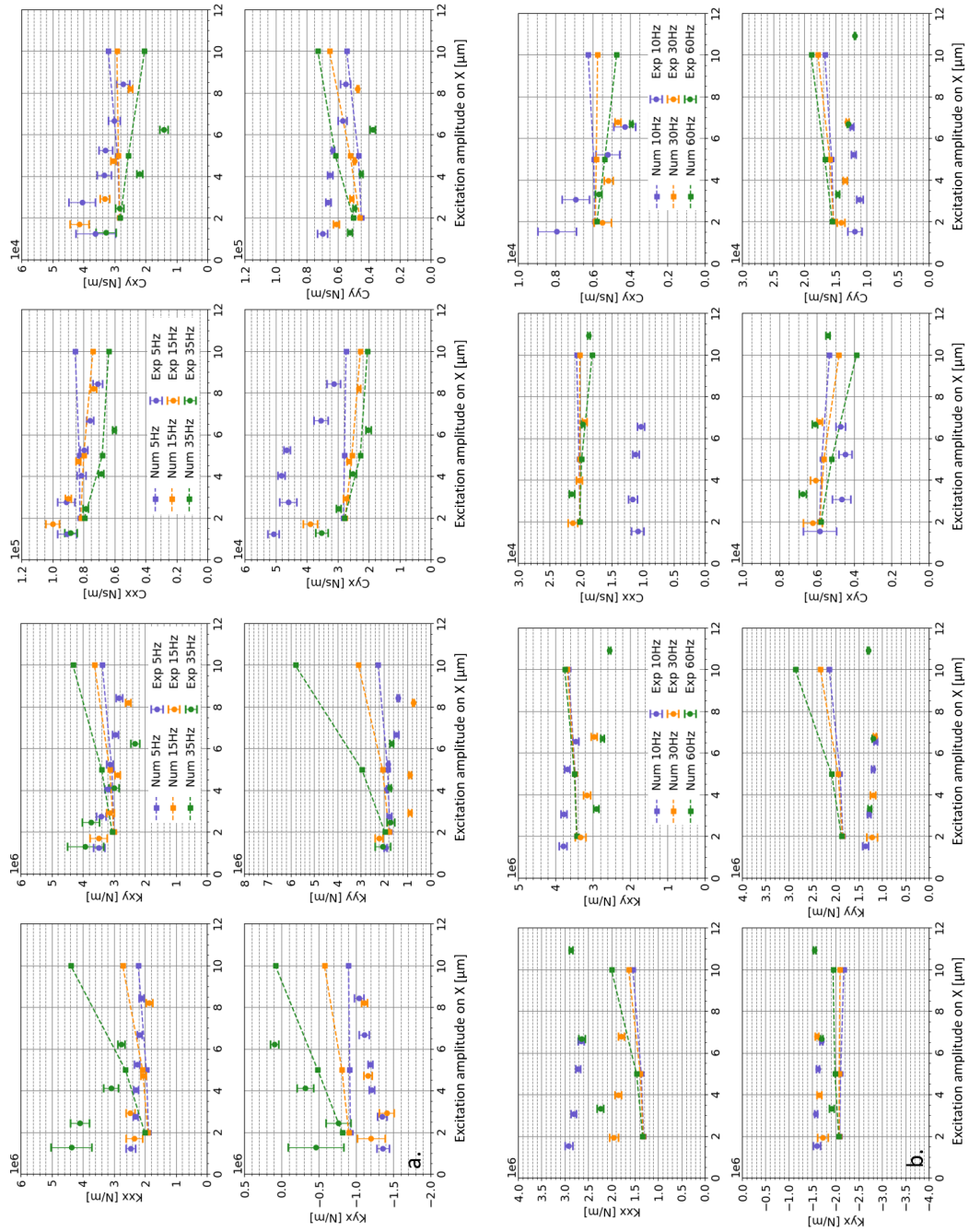

Figure 7: Dynamic coefficients of the plain journal bearing at: a. 600 rpm. b. 3000 rpm.

The experimental results obtained for tilting pad journal bearing were compared with numerical predictions developed by [1]. The Figure 8a. presents the experimental identification of the dynamic coefficients for a rotational speed of 600 rpm (10 Hz), an excitation frequency of 15 Hz (1.5X) and for several X excitation amplitudes. The stiffness and the direct damping coefficients don't show much variation with the excitation amplitude. The cross-coupled damping shows a weak variation with the excitation amplitude. These results show that the excitation amplitude don't influence the dynamic coefficients.

Figures 8b. and 9 present the dynamic coefficients for rotation speeds of 600, 3000 and 7200 rpm and several excitation frequencies. In these tests, the excitation amplitudes were kept between 5 and 10 µm. The numerical calculations were performed for several geometries of tilting pad journal bearing, in order to observe the impact of bearing geometry (especially its pad clearance, C_r and preload, a) on the dynamic coefficients:

- Theoretical geometry. C_r=75 µm, a=25 µm
- Measured geometry, C_r=100 µm, a=50 µm
- Variation preload 1, C_r=100 µm, a=30 µm
- Variation preload 2, C_r=100 µm, a=10 µm

The measured geometry is an average of a 3D measurement of each pad (Pad 1: C_r=102.3 µm, a=50.1 µm; Pad 2: C_r=83.1 µm, a=31 µm; Pad 3: C_r=10; Pad 4: C_r=111.2 µm, a=62.5 µm) as it was not possible to add the individual characteristics of each pad in the numerical modelling;

Experimentally, for each speed, the coefficients identified from sub-synchronous excitations (excitation at 5 Hz for 600 rpm, at 10 and 30 Hz for 3000 rpm and 30 and 90 Hz for 7200 rpm) appear to have a larger standard deviations than coefficients identified from super-synchronous excitations. In addition, the values obtained are sometimes far apart, for example the coefficients Cxy and Cyx at 5 Hz and 600 rpm.

In the case of theoretical geometry, the direct stiffness and damping coefficients are greater than those obtained experimentally. For the measured geometry, the same observation can be made. For the other two geometries, with a different preload, the direct numerical coefficients approach the experimental coefficients. The last case with a preload of 10 µm shows the best correlation. However, the modifications of the machining radial clearance and the preload have little influence on the cross coupling terms which in the majority of cases remain far from the values identified experimentally.

5 Discussion

This paper presents the use of an EMA to identify the dynamic coefficients of fluid film bearings. The main points are:

1. The use of a modified force-current formulation to taking into account the defects of machining and positioning
2. The in-situ calibration of the EMA
3. The experimental identification of a plain journal bearing.
4. The experimental identification of a tilting pad journal bearing.

The first point shows an improvement on the knowledge of the initial important parameters, nevertheless, the in-situ calibration shows error on transverse moment of inertia at up to 12%. This prove that the in-calibration can still be improved.

Regarding the plain bearing, the results for the two rotational speeds tested are on the whole conclusive with a good adequacy of the numerical and experimental values. This validates the use of

the digital model to calculate the dynamic coefficients of the bearing in other configurations (static load, speed of rotation).

For the tilting pad journal bearing, the experimental results does not agree well with numerical modelling. Several authors [8, 7, 6, 4] have underlined the influence of machining tolerances on the static characteristics and dynamic coefficients of tilting pad bearings and in particular the importance of the radial machining clearance and preload. For example, the fact that the two measured cross-coupling stiffness coefficients are positive seems to come from the fact that all the pads are different because of their respective faults, in particular pads 2 and 4 which have very different preloads and radial clearances. In a future study, it would be interesting to implement the faults of each pad in the numerical computer code to thus verify this hypothesis.

To conclude, there is a significant level of uncertainty arising from the conformity of the digital model with reality (mainly due to the excitation method), from the indirect measurement of the current and therefore from the calculation of the force, despite the calibration performed. In the future, it would be interesting to identify the dynamic coefficients for other speeds over the entire operating range of the test bench. The integration of Hall effect sensors, in order to directly measure the effort, would reduce the level of uncertainty in the results. In terms of the digital model, it would be also interesting to test several models of cavitation.

6 Acknowledgements

The authors acknowledge the work of Geoffrey Habasque on the design of the EMA during his final year project at INSA Lyon.

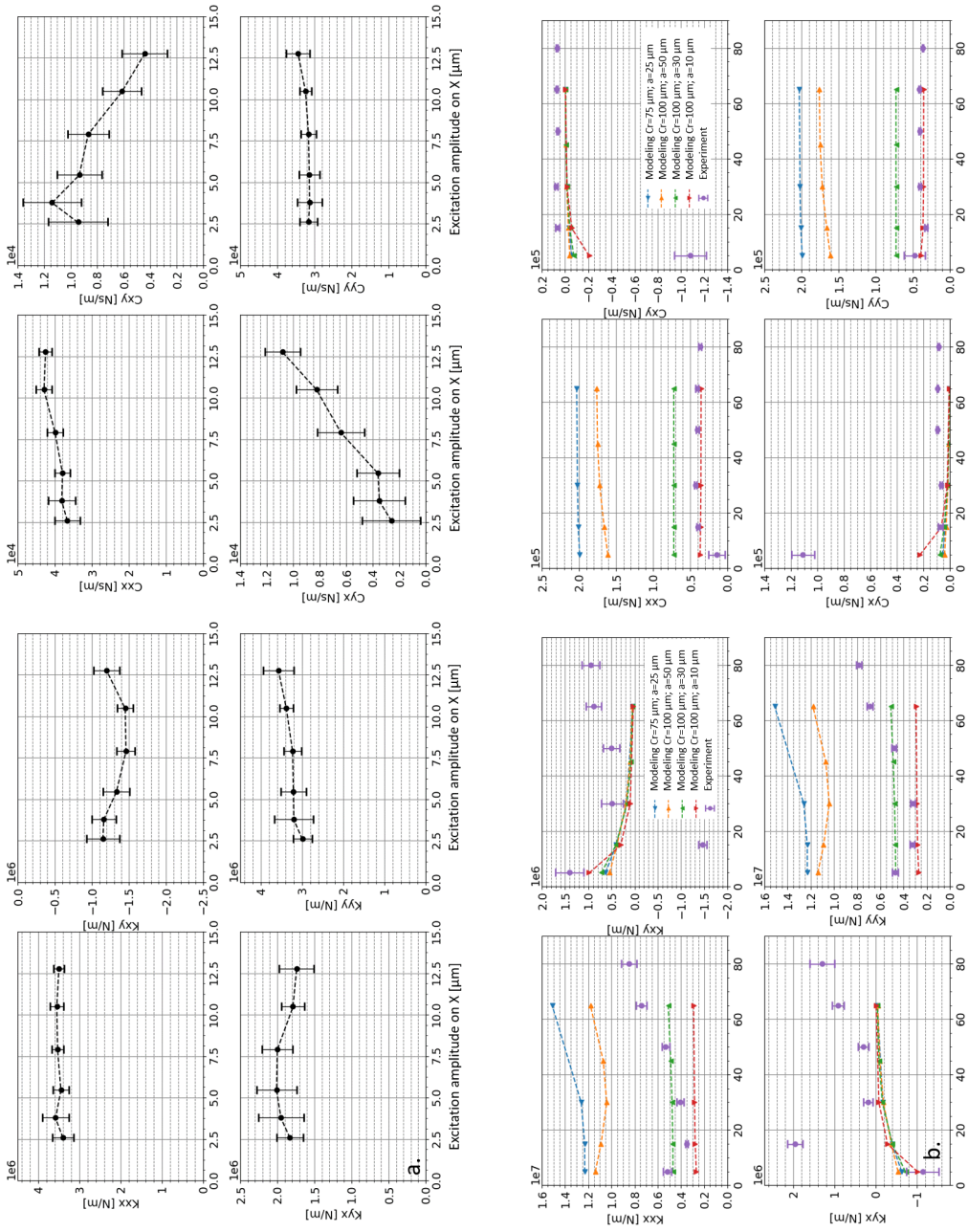

Figure 8: Dynamic coefficient of the tilting pad journal bearing at 600 rpm. a. Function of amplitude for an excitation of 15 Hz. b. Comparison with numerical modelling with various clearances and preloads.

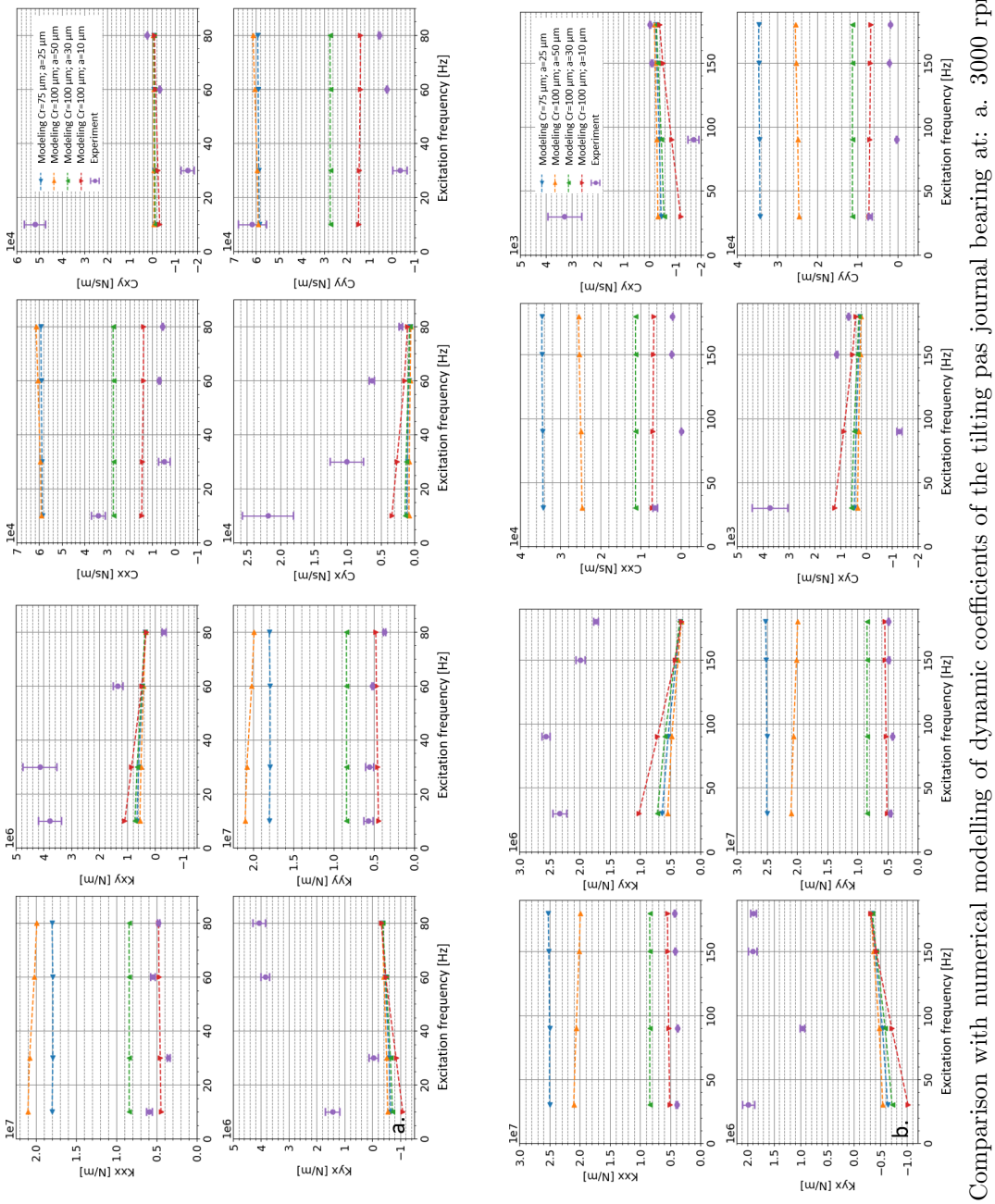

Figure 9: Comparison with numerical modelling of dynamic coefficients of the tilting pas journal bearing at: a. 3000 rpm. b. 7200 rpm.

References

[1] M. Arghir. Étude de faisabilité de paliers à patins oscillants et de butées fluides pour turbopompes spatiales, 2017. Accord spécifié de collaboration de recherche CNES W.160753/00, contrat CNRS 785596.

[2] P. Arumugam, S. Swarnamani, and B.S. Prabhu. Experimental Identification of Linearized Oil Film Coefficients of Cylindrical and Tilting Pad Bearings. *J. Eng. Gas Turbines Power*, 117:33–40, 1995.

[3] E. Bellabarba, S. Díaz, and V. Rastelli. A Test Rig for Air Bearings Rotordynamic Coefficients Measurement. In *ASME Turbo Expo 2005 Power Land, Sea Air*, pages 1–7, 2005.

[4] P.V. Dang, S. Chatterton, P. Pennacchi, and A. Vania. Numerical Investigation of the Effect of Manufacturing Errors in Pads on the Behaviour of Tilting-Pad Journal Bearings. *Proc. Inst. Mech. Eng. Part J J. Eng. Tribol.*, 232(4):480–500, 2017.

[5] T.W. Dimond, P.N. Sheth, P.E. Allaire, and M. He. Identification Methods and Test Results for Tilting Pad and Fixed Geometry Journal Bearing Dynamic Coefficients - A Review. *Shock Vib.*, 16(1):13–43, 2009.

[6] W. Dmochowski, A. Dadouche, and M. Fillon. Numerical Study of the Sensitivity of Tilting-Pad Journal Bearing Performance Characteristics to Manufacturing Tolerances : Dynamic Analysis. *Tribol. Trans.*, 51(5):573–580, 2008.

[7] M. Fillon, W. Dmochowski, and A. Dadouche. Numerical Study of the Sensitivity of Tilting Pad Journal Bearing Performance Characteristics to Manufacturing Tolerances : Steady-State Analysis. *Tribol. Trans.*, 50(3):387–400, 2007.

[8] G.J. Jones and F.A. Martin. Geometry Effects in Tilting-Pad Journal Bearings. *Tribol. Trans.*, 22(3):227–244, 1979.

[9] E. Knopf and R. Nordmann. Active magnetic bearings for the identification of dynamic characteristics of fluid bearings: calibration result. In *6th Int. Symp. Magnetic Bearing, Cambridge, Massachusetts*, 1998.

[10] E. Knopf and R. Nordmann. Identification of the dynamic characteristics of turbulent journal bearings using active magnetic bearings. In *7th Int. Conf. Vib. Rot. Mach., Nottingham, GB*, 2000.

[11] T. Plantegenet, M. Arghir, M-A. Hassini, and P. Jolly. The thermal unbalance effect induced by a journal bearing in rigid and flexible rotors: Experimental analysis. *Tribology Transactions*, 63(1):52–67, 2020.

[12] T. Plantegenet, M. Arghir, and P. Jolly. Experimental analysis of the thermal unbalance effect of a flexible rotor supported by a flexure pivot tilting pad bearing. *Mechanical Systems and Signal Processing*, 145:106953, 2020.

[13] S.K. Reddy, S. Swarnamani, and B.S. Prabhu. Experimental Investigation on the Performance Characteristics of Tilting Pad Journal Bearings for Small L/D Ratios. *Wear*, 212:33–40, 1997.

[14] G. Schweitzer and E.H. Maslen. *Magnetic Bearings : Theory, Desing, and Application to Rotating Machinery*. 2009.

[15] R. Tiwari, A.W. Lees, and M.I. Friswell. Identification of Dynamic Bearing Parameters: A Review. *Shock Vib. Dig.*, 36(2):99–124, 2004.

[16] A.J. Voigt. *Towards Identification of Rotordynamic Properties for Seals in Multiphase Flow Using Active Magnetic Bearings Design and Commissioning of a Novel Test Facility*. PhD thesis, Technical University of Denmark, 2016.